

Segmental Hidden Markov Models with Random Effects for Waveform Modeling

Seyoung Kim

*Department of Computer Science
University of California, Irvine
Irvine, CA 92697-3425, USA*

SYKIM@ICS.UCI.EDU

Padhraic Smyth

*Department of Computer Science
University of California, Irvine
Irvine, CA 92697-3425, USA*

SMYTH@ICS.UCI.EDU

Editor: Sam Roweis

Abstract

This paper proposes a general probabilistic framework for shape-based modeling and classification of waveform data. A segmental hidden Markov model (HMM) is used to characterize waveform shape and shape variation is captured by adding random effects to the segmental model. The resulting probabilistic framework provides a basis for learning of waveform models from data as well as parsing and recognition of new waveforms. Expectation-maximization (EM) algorithms are derived and investigated for fitting such models to data. In particular, the “expectation conditional maximization either” (ECME) algorithm is shown to provide significantly faster convergence than a standard EM procedure. Experimental results on two real-world data sets demonstrate that the proposed approach leads to improved accuracy in classification and segmentation when compared to alternatives such as Euclidean distance matching, dynamic time warping, and segmental HMMs without random effects.

Keywords: waveform recognition, random effects, segmental hidden Markov models, EM algorithm, ECME

1. Introduction

Automatically parsing and recognizing waveforms based on their shape has broad applications, including interpretation and classification of heartbeats in ECG data analysis (Koski, 1996), analysis of waveforms from turbulent flow experiments (Bruun, 1995), and discrimination of nuclear events and earthquakes in seismograph data (Bennett and Murphy, 1986). Waveform analysis has also attracted attention in information retrieval and data mining, with a focus on algorithms that can take a waveform as an input query and search a large database to find similar waveforms that match the query waveform (e.g., Yi and Faloutsos, 2000). Applications include finding temporal patterns in retail time-series data (Agrawal et al., 1993) and fault diagnosis in complex systems (Keogh and Smyth, 1997).

While the human visual system can easily recognize the characteristic signature of a particular waveform shape (a heartbeat waveform for example) the problem can be quite difficult for automated methods. For example, Figure 1 shows a set of time-series waveforms collected during turbulent fluid-flow experiments where the shape of each waveform is determined by the nature of

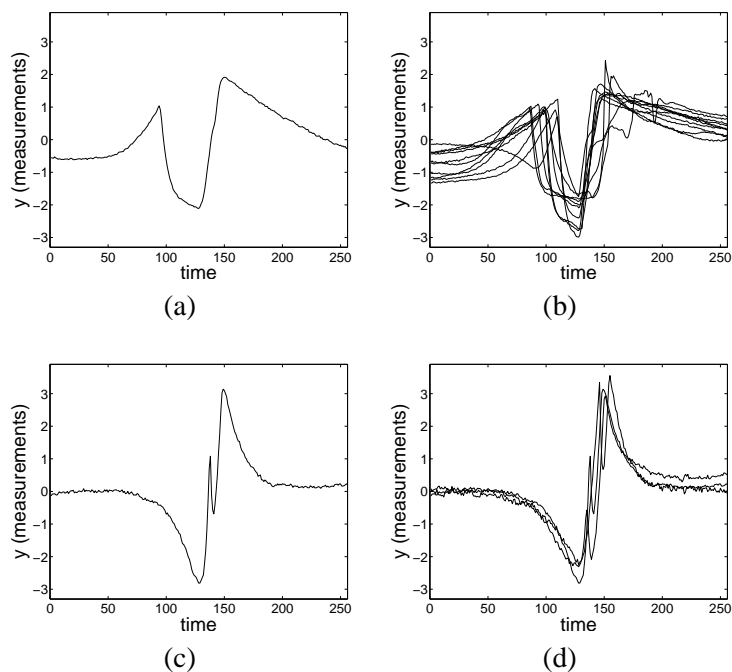


Figure 1: Fluid-flow waveform data: (a) a waveform from the class *splitting* (where the probe splits a bubble), (b) a set of such waveforms, (c) a waveform from the class *glance*, and (d) a set of such waveforms.

interactions between a probe and bubbles in the fluid. Figure 1(a) shows an example waveform from a particular type of interaction. Figure 1(b) shows a whole set of such waveforms that have all been classified (by human experts) as being of the same interaction type. Although all of these waveforms belong to the same interaction class, there is significant variability in shape among those waveforms. The sources of variability include shifts of the locations of prominent features such as peaks, valleys, and plateaus, scaling along the time and amplitude axes, and measurement noise. An example waveform from a different class is shown in Figure 1(c), and a set of such waveforms are shown in Figure 1(d). Again there is significant within-class variability.

In this paper we address the problem of detecting and classifying general classes of waveforms based on their shape and propose a new statistical model that directly addresses within-class shape variability. We will assume in the paper that the waveforms to be analyzed are in the form of “snippets” that have already been extracted from the “background” time-series, e.g., in the form of Figures 1(b) and (d). This assumption can be relaxed—we outline a method for detection of waveforms that are embedded in a time-series in Section 6. We will also assume that the waveforms are being analyzed offline, i.e., that all of the waveform measurements are available at the time of analysis rather than arriving sequentially in an online fashion. The online sequential detection problem can be addressed by generalizing the methods we propose, but we do not pursue online algorithms in this paper.

We will assume that a set of one or more waveforms from a single class are provided a priori (e.g., the data in Figures 1(b) or (d)) and from this data we wish to learn a model for recognition. Hidden Markov models (HMMs) are a broadly useful class of generative models for waveform

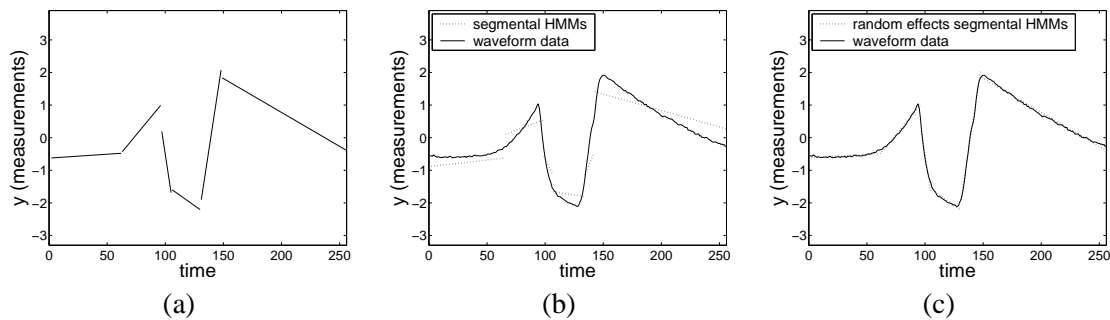


Figure 2: Waveform models: (a) a piecewise linear approximation of the waveform in Figure 1(a), (b) a segmental HMM best fit, and (c) a random effects segmental HMM best fit as described in this paper.

modeling, finding application (for example) in heartbeat monitoring of ECG data (Koski, 1996; Hughes et al., 2003). These models are characterized by (a) a discrete-time finite-state Markov process which is unobserved, and (b) a set of observed measurements at each time t which only depend (stochastically) on the state value at time t . From a shape-modeling viewpoint the standard version of the model generates noisy versions of piecewise constant shapes over time, since the observations within a sequence of states of the same value have constant mean. For waveform modeling, a useful extension is the so-called segmental HMM, originally introduced in the speech recognition (Russell, 1993) and more recently used for more general waveform modeling (Ge and Smyth, 2000). The segmental model allows for the observed data within each segment (a sequence of states with the same value) to follow a general parametric regression form, such as a linear function of time with additive noise. This allows us to model the shape of the waveform directly, in this case as a sequence of piecewise linear components—Figure 2(a) shows a piecewise linear representation of the waveform in Figure 1(a).

A limitation of this particular model is that it assumes that the parameters of the model are fixed. Thus, the only source of variability in an observed waveform arises from variation in the lengths of the segments and observation noise added to the functional form in each segment. The limitation of this can clearly be seen in Figure 2(b), where a segmental HMM has been trained on the data in Figure 1(b) and then used to generate maximum-likelihood estimates of segment boundaries, slopes, and intercepts for the new waveform in Figure 2(b). We can see that the best-fit slopes and intercepts provided by the model do not match the observed data particularly well in each segment, e.g., in the first segment the intercept is clearly too low on the y -axis, in the second segment the slope is too small, and so forth. By using the same fixed parameters for all waveforms, the model cannot fully account for variability in waveform shapes (e.g., as seen in Figure 1(b)).

To address this limitation, in this paper we combine segmental HMMs with random effects models. The general idea of random effects is to allow each group of observations (or each waveform) to have its own parameters that are still coupled together by an overall population prior (Laird and Ware, 1982). By extending the segmental HMM to include random effects, we can allow the slopes and intercepts within each segment of each waveform to vary according to a prior distribution. As illustrated in Figure 3, in the hierarchical setup of our model each waveform (at the bottom level) has its own slope and intercept parameters (as shown at the middle level) that come from a shape

template (at the top level) modeled as a population prior. The parameters of this prior can be learned in an unsupervised manner from data in the form of sets of waveforms. The resulting model can be viewed as a directed graphical model, allowing for application of standard methods for inference and learning (Jordan, 1999; Murphy, 2002). For example, we can in principle learn that the slopes across multiple waveforms for the first segment in Figure 1(b) tend to have a characteristic mean slope and standard deviation. The random effects approach provides a systematic mechanism for allowing variation in “shape space” in a manner that can be parametrized. Figure 2(c) shows a visual example of how a random effects model (constructed from the training data in Figure 1(b)) is used to generate maximum-likelihood estimates of segment boundaries and segment slopes and intercepts for the waveform in Figure 1(a).

Kim et al. (2004) described preliminary results using random effects segmental HMMs for waveform parsing and recognition. A drawback of this earlier approach is the relatively slow convergence of the expectation-maximization (EM) algorithm in learning. This is a result of the large amount of missing information present (due to the random effects component of the model), compared to a standard segmental HMM. In this paper we use the “expectation conditional maximization either” (ECME) algorithm (Liu and Rubin, 1994) for parameter estimation of random effects segmental HMMs. This dramatically speeds up convergence relative to the EM algorithm, making the model much more practical to use for real-world waveform recognition problems.

We begin our discussion by reviewing related work on segmental HMMs and random effects models in Section 2. We introduce segmental HMMs in Section 3. In Section 4, we extend this model to incorporate random effects models, and describe the inference procedure and the EM algorithm for parameter estimation. We also show that the ECME algorithm can be used to significantly speed up the convergence of the EM algorithm. In Section 5, we evaluate our model on two applications involving bubble-probe interaction data and ECG data, and compare random effects segmental HMMs to other waveform-matching algorithms such as Euclidean distance matching, dynamic time warping, and segmental HMMs without random effects. Section 6 contains a brief discussion of possible extensions of the model and final conclusions.

2. Related Work and Contributions

A general approach to waveform recognition is to extract characteristic features from the waveform in the time-domain or the frequency-domain, and then perform classification in the resulting feature-vector space. Examples of this approach include the work of Shimshoni and Intrator (1998) who used neural networks to classify seismic waveforms, and Jankowski and Oreziak (2003) who used support vector machines to classify heartbeats in ECG data. Using classifiers in this manner requires training data from both positive and negative classes as well as the extraction of reliable discriminative features from the raw waveform data. In the approach described in this paper we avoid these requirements by learning models from the positive class only and by modeling the waveform directly in the time-domain without any need for feature extraction. Other techniques have been pursued in the area of waveform query-matching for information retrieval involving time-series data (e.g., Agrawal et al., 1993; Chan and Fu, 1999; Keogh and Pazzani, 2000; Yi and Faloutsos, 2000). These approaches generally focus on the investigation of robust and computationally efficient similarity measures. In contrast, in this paper, we focus on a generative model approach, allowing techniques from statistical learning to be brought to bear. This allows us (for example)

to learn models from data, to handle within-class waveform variability, and to generate maximum-likelihood segmentations of waveforms.

As mentioned in Section 1, standard discrete-time finite-state HMMs are not ideal for modeling waveform shapes since the generative model implicitly assumes a geometric distribution on segment lengths and a piecewise constant shape model. Segmental HMMs relax these modeling constraints by allowing (a) arbitrary distributions on run lengths, and (b) “segment models” (regression models) that allow the mean to be a function of time within each segment. HMMs that allow arbitrary distributions on run lengths (the semi-Markov property in a HMM context) were introduced in the work of Ferguson (1980), Russell and Moore (1985), and Levinson (1986). Deng et al. (1994) and Russell (1993) extended these models to segmental HMMs by modeling dependencies between observations from the same state with a parametric trajectory model that changes over time. Ostendorf et al. (1996) reviewed variations of segmental HMMs from a speech recognition perspective. More recent work includes Achan et al. (2005) and Yun and Oh (2000). Ge and Smyth (2000) introduced the idea of using segmental HMMs for general waveform recognition problems.

The idea of using random effects with segmental HMMs to model parameter variability across waveforms is implicit in the speech recognition work of both Gales and Young (1993) and, later, Holmes and Russell (1999). This work can be viewed as precursors to the more general random effects segmental HMM framework we present in this paper. Gales and Young (1993) used a model with a constant mean per segment, but where the mean values themselves come from a distribution, allowing modeling of variability across different individual speakers. Holmes and Russell (1999) extended this idea to use a linear regression function instead of a constant mean for each segment with a Gaussian prior on the regression parameters (slope and intercept) for each segment. In earlier work (Kim et al., 2004), we noted that Holmes and Russell’s model could be formalized within a random effects framework, and derived a more general EM framework for such models, taking advantage of ideas developed separately in speech recognition and in statistics.

In the statistical literature there is a significant body of work on modeling a hierarchical data-generating process with a random effects model and estimating the parameters of this model (Searle et al., 1992). Dempster et al. (1977) sketched the EM algorithm for finding maximum-likelihood estimates for parameters of random effects models. This algorithm was further developed by Dempster et al. (1981), Laird and Ware (1982), and Laird et al. (1987). There appears to be no work in the statistical literature on applying random effects to segmental HMMs.

In this context, the primary contribution of this paper is a general framework for random-effects segmental hidden Markov models. We demonstrate how such models can be used for waveform modeling, recognition, and segmentation, with experimental comparisons of the random effects approach with alternative methods such as dynamic time warping, using two real-world data sets. We extend earlier approaches for learning the parameters of random effects segmental HMMs by deriving a provably correct EM algorithm with monotonic convergence. Both Gales and Young (1993) and Holmes and Russell (1999) derived EM-like optimization algorithms, but their M steps are not in a closed form and use approximate solutions—thus, the monotonic convergence property of EM is not guaranteed in general using their approaches.

We further extend the standard EM algorithm to develop an ECME algorithm for fitting random effects segmental HMMs. The ECME approach significantly reduces the number of iterations required for convergence, relative to EM, while increasing the time complexity per iteration only slightly. For example, as we will discuss later, ECME led to a time-savings of 3 orders of magnitude over the standard EM approach in our experiments. We derive a computationally efficient

inference algorithm (applicable to both EM and ECME) that reduces the time complexity of the forward-backward algorithm by a factor of T^2 , where T is the length of a waveform. We also show that this inference algorithm can be applied to full covariance models rather than assuming (as in Holmes and Russell, 1999) that the intercept and slope in the segment distribution are conditionally independent. Since the inference algorithm is used in each iteration of the E step in the EM and ECME iterations, this significantly reduces the overall time complexity of each iteration of EM and ECME.

3. Segmental HMMs

A segmental HMM with M states is described by an $M \times M$ transition matrix, a probability distribution over duration for each state, and a segment model for each state. The transition matrix \mathbf{A} (assumed here to be stationary in time) has entries a_{kl} , namely, the probability of being in state l at time $t + 1$ given state k at time t . The initial state distribution can be included in \mathbf{A} as transitions from a special state 0 to each state $k = 1, \dots, M$. In waveform modeling, we typically constrain the transition matrix to allow only left-to-right transitions and do not allow self-transitions. Thus, there is an ordering on states, each state can be visited at most once, and states can be skipped.

In this paper, we model the duration distribution of state k using a Poisson distribution,

$$P(d-1|\lambda_k) = \frac{e^{-\lambda_k} \lambda_k^{d-1}}{(d-1)!} \quad d = 1, 2, \dots$$

(shifted to start at $d = 1$ to prevent a silent state). Other choices for the duration distribution could also be used (e.g., Ferguson, 1980; Levinson, 1986). Once the process enters state k , a duration d is drawn, and state k produces a segment of observations of length d from the segment distribution model. In this paper we focus on models with linear functional forms within each segment. We model the r th segment of observations of length d , \mathbf{y}_r , generated by state k , as a linear function of time,

$$\mathbf{y}_r = \mathbf{X}_r \boldsymbol{\beta}_k + \mathbf{e}_r \quad \mathbf{e}_r \sim N_d(\mathbf{0}, \sigma^2 \mathbf{I}_d), \quad (1)$$

where $\boldsymbol{\beta}_k$ is a 2×1 vector of regression coefficients for the intercept and slope, \mathbf{e}_r is a $d \times 1$ vector of Gaussian noise with variance σ^2 for each component, and \mathbf{X}_r is a $d \times 2$ design matrix consisting of a column of 1's (for the intercept term) and a column of x values representing discrete time values.

In speech recognition using the mid-point of a segment as a parameter in the model instead of intercept has been shown to lead to better speech recognition performance (Holmes and Russell, 1999). Nonetheless, parametrization of the model via the intercept worked well in our experiments, and for this reason we use the intercept in the models discussed in this paper. For simplicity, σ^2 is assumed to be common across all states; again this can be relaxed. We do not enforce continuity of the mean functions (Equation (1)) across segments in the probabilistic model. However, as reported in Section 5, the model without continuity constraints worked well on real-world data in our recognition experiments.

Treating the unobserved state sequences as missing, we can estimate the parameters, $\theta = \{\mathbf{A}, \Lambda = \{\lambda_k | k = 1, \dots, M\}, \theta_f = \{\boldsymbol{\beta}_k, (\sigma^2) | k = 1, \dots, M\}\}$, using the EM algorithm, with the forward-backward (F-B) algorithm as a subroutine for inference in the E step (Deng et al., 1994). The F-B algorithm for segmental HMMs, modified from that of standard HMMs to take into account the duration dis-

tribution, recursively computes

$$\begin{aligned}\alpha_t(k) &= P(y_{1:t}, \text{state } k \text{ ends at } t | \theta) \\ \alpha_t^*(k) &= P(y_{1:t}, \text{state } k \text{ starts at } t + 1 | \theta)\end{aligned}\quad (2)$$

in the forward pass, and

$$\begin{aligned}\beta_t(k) &= P(y_{t+1:T} | \text{state } k \text{ ends at } t, \theta) \\ \beta_t^*(k) &= P(y_{t+1:T} | \text{state } k \text{ starts at } t + 1, \theta)\end{aligned}\quad (3)$$

in the backward pass, and returns the results to the M step as a set of sufficient statistics (Rabiner and Juang, 1993).

Inference algorithms for segmental HMMs provide a natural way to evaluate the performance of the model on test data. The F-B algorithm scores a previously unseen waveform \mathbf{y} by calculating the likelihood

$$p(\mathbf{y} | \theta) = \sum_{\mathbf{s}} p(\mathbf{y}, \mathbf{s} | \theta) = \sum_k \alpha_T(k), \quad (4)$$

where \mathbf{s} represents a sequence of unknown state labels for observations \mathbf{y} . The Viterbi algorithm can provide a segmentation of a waveform by computing the most likely state sequence (e.g., Figure 2(b)). The addition of duration distributions in segmental HMMs increases the time complexity of both the F-B and Viterbi algorithms from $O(M^2T)$ for standard HMMs to $O(M^2T^2)$, where T is the length of the waveform (i.e., the number of observations).

4. Segmental HMMs with Random Effects

A random effects model is a general statistical framework when the data generation process has a hierarchical structure, coupling a population-level model with individual-level variation. At each level of the generative process, the model defines a prior distribution over the individual group parameters, called random effects, of one level below. The observed data are generated at the bottom of the hierarchy, given parameters drawn from the prior distribution one level above. Typically, the random effects are not observable, so the EM algorithm is a popular approach to learning model parameters from the observed data (Dempster et al., 1981; Laird and Ware, 1982). By combining segmental HMMs and random effects models we can take advantage of the strength of each in waveform modeling. Random effects models add one level of hierarchy to the probabilistic structure of segmental HMMs, defining a population distribution over the possible shapes of waveform segments. Instead of requiring all waveforms to be modeled with a single set of parameters, individual waveforms are allowed to have their own parameters but coupled by a common population prior across all waveforms.

4.1 The Model

Beginning with the segmental HMMs described in Section 3, we add random effects via a new variable \mathbf{u}_r^i to the segment distribution part of the model as follows. Consider the r th segment \mathbf{y}_r^i of length d from the i th individual waveform \mathbf{y}^i generated by state k . Following the discussion in Laird

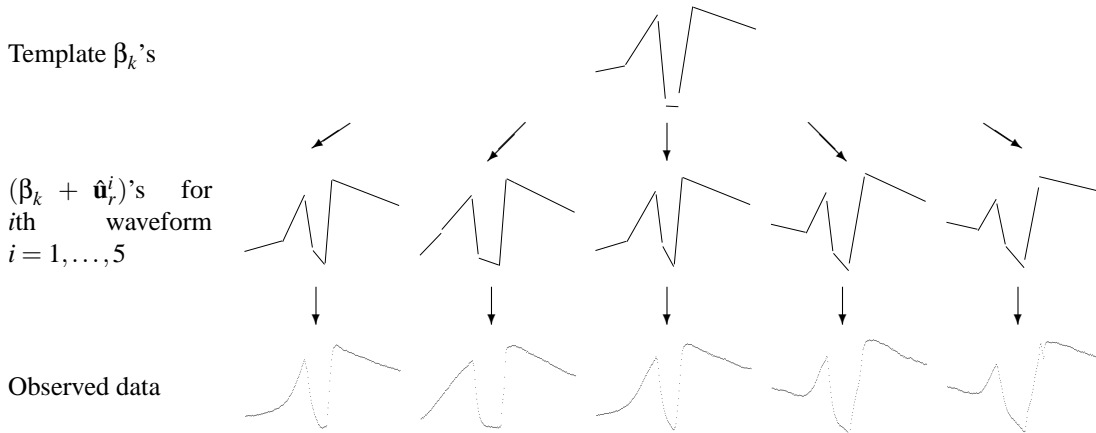


Figure 3: A visual illustration of the random effects segmental HMM, using fluid-flow waveform data as an example (as described in Section 5.1). The top level shows the population level parameters β_k 's for the waveform shape. The plots at the bottom level consist of observed data. The plots in the middle level show the posterior estimates (combining both the data and the prior) of $\hat{\mathbf{u}}^i$ and $\hat{\mathbf{s}}^i$, using Equation (8) and the Viterbi algorithm respectively.

and Ware (1982), we describe the generative model as a two-level process. At the bottom level, we model the observed data \mathbf{y}_r^i as

$$\mathbf{y}_r^i = \mathbf{X}_r^i \beta_k + \mathbf{X}_r^i \mathbf{u}_r^i + \mathbf{e}_r^i \quad \mathbf{e}_r^i \sim N_d(\mathbf{0}, \sigma^2 \mathbf{I}_d), \quad (5)$$

where \mathbf{e}_r^i is the measurement noise, \mathbf{X}_r^i is a $d \times 2$ design matrix for the time measurements corresponding to \mathbf{y}_r^i , $(\beta_k + \mathbf{u}_r^i)$ are the regression coefficients, and $1 \leq i \leq N$ (for N waveforms). β_k represents the mean regression parameters for segment k , and \mathbf{u}_r^i represents the variation in regression (or shape) parameters for the i th individual waveform. At this level, the individual random effects \mathbf{u}_r^i as well as β_k and σ^2 are viewed as parameters. At the top level, \mathbf{u}_r^i is viewed as a random variable with distribution

$$\mathbf{u}_r^i \sim N_2(\mathbf{0}, \Psi_k), \quad (6)$$

where Ψ_k is a 2×2 covariance matrix, and \mathbf{u}_r^i is independent of \mathbf{e}_r^i . Notice that this model described by Equations (5) and (6) is equivalent to having $\mathbf{y}_r^i = \mathbf{X}_r^i \beta_r^i + \mathbf{e}_r^i$ with $\beta_r^i \sim N_2(\beta_k, \Psi_k)$. It can be shown that \mathbf{y}_r^i and \mathbf{u}_r^i have the following joint distribution:

$$\begin{pmatrix} \mathbf{y}_r^i \\ \mathbf{u}_r^i \end{pmatrix} \sim N_{d+2} \left(\begin{pmatrix} \mathbf{X}_r^i \beta_k \\ \mathbf{0} \end{pmatrix}, \begin{pmatrix} \mathbf{X}_r^i \Psi_k \mathbf{X}_r^{i'} + \sigma^2 \mathbf{I}_d & \mathbf{X}_r^i \Psi_k \\ \Psi_k \mathbf{X}_r^{i'} & \Psi_k \end{pmatrix} \right). \quad (7)$$

Also, from Equation (7), the posterior distribution of \mathbf{u}_r^i can be written as

$$\mathbf{u}_r^i | \mathbf{y}_r^i, \beta_k, \Psi_k, \sigma^2 \sim N_2(\hat{\mathbf{u}}_r^i, \Psi_{\hat{\mathbf{u}}_r^i}), \quad (8)$$

where

$$\hat{\mathbf{u}}_r^i = (\mathbf{X}_r^{i'} \mathbf{X}_r^i + \sigma^2 (\Psi_k)^{-1})^{-1} \mathbf{X}_r^{i'} (\mathbf{y}_r^i - \mathbf{X}_r^i \beta_k), \quad (9)$$

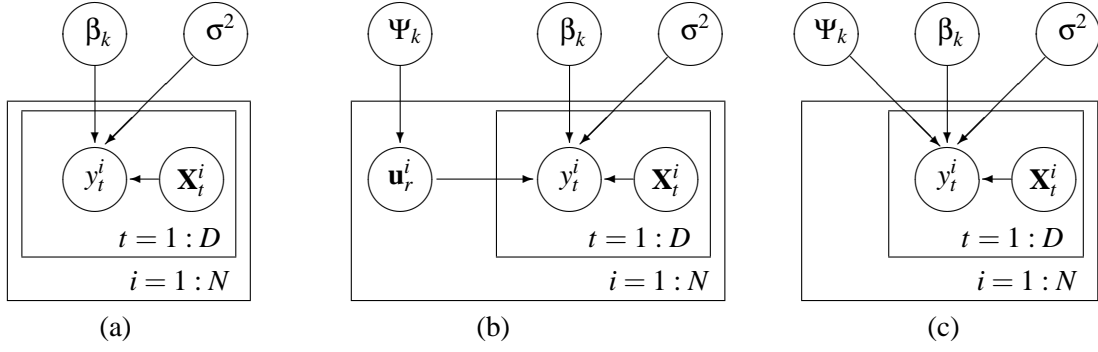


Figure 4: Plate diagrams for the segment distribution part of segmental HMMs and random effects segmental HMMs. (a) segment model in segmental HMMs, (b) a two-stage model with random effects parameters in random effects segmental HMMs, and (c) the model after integrating out random effects parameters from (b).

and

$$\Psi_{\hat{\mathbf{u}}_r^i} = \sigma^2 (\mathbf{X}_r^i \mathbf{X}_r^i + \sigma^2 (\Psi_k)^{-1})^{-1}. \quad (10)$$

In the discussion that follows we use \mathbf{u}^i to denote $\{\mathbf{u}_r^i | r = 1, \dots, R\}$ given the segmentation \mathbf{s}^i of waveform \mathbf{y}^i into R segments. Similarly, $\hat{\mathbf{u}}^i$ represents $\{\hat{\mathbf{u}}_r^i | r = 1, \dots, R\}$, given the segmentation $\hat{\mathbf{s}}^i$ of waveform \mathbf{y}^i found by the Viterbi algorithm.

Figure 3 conceptually illustrates the hierarchical setup of the model. The shape template described by the population parameters β_k 's is shown at the top of the hierarchy. The plots at the bottom level consist of observed data. The plots at the middle level show the posterior estimates (combining both the data and the prior) of $\hat{\mathbf{u}}^i$ and $\hat{\mathbf{s}}^i$, using Equation (8) and the Viterbi algorithm respectively. From a generative model perspective, the shape templates in the middle row, $(\beta_k + \mathbf{u}_r^i)$'s, $i = 1, \dots, 5$, are generated from the mean shape at the top level by Equation (6). The observed data at the bottom of the hierarchy are modeled as noisy realizations of these individual shape templates. This final data generation process is modeled in Equation (5).

Figure 4 shows plate diagrams for the segment distribution part of segmental HMMs and random effects segmental HMMs, illustrating the generative process for N waveforms, $\mathbf{y}^1, \dots, \mathbf{y}^N$, under the simplifying assumption that each waveform comes from a single segment of length D corresponding to state k .

4.2 Inference

To handle the random effects component in the F-B and Viterbi algorithms for segmental HMMs, we notice from Equation (7) that the marginal distribution of a segment \mathbf{y}_r^i generated by state k is $N_d(\mathbf{X}_r^i \beta_k, \mathbf{X}_r^i \Psi_k \mathbf{X}_r^{i'} + \sigma^2 \mathbf{I}_d)$, and that this corresponds to Equation (1) with the covariance matrix $\sigma^2 \mathbf{I}_d$ replaced by $(\mathbf{X}_r^i \Psi_k \mathbf{X}_r^{i'} + \sigma^2 \mathbf{I}_d)$. Replacing the two-level segment distribution with this marginal distribution, and collapsing the hierarchy into a single level, we can use the same F-B and Viterbi algorithm as in segmental HMMs in the marginalized space over the random effects parameters \mathbf{u}^i .

The F-B algorithm recursively computes the quantities in Equations (2) and (3). These are then used in the M step of the EM algorithm. The likelihood of a waveform \mathbf{y} , given fixed parameters $\theta = \{\mathbf{A}, \Lambda, \theta_f = \{\beta_k, \Psi_k, (\sigma^2) | k = 1, \dots, M\}\}$, but with states \mathbf{s} and random effects \mathbf{u} unknown, is evaluated as

$$\begin{aligned} p(\mathbf{y}|\theta) &= \sum_{\mathbf{s}} \int p(\mathbf{y}, \mathbf{s}, \mathbf{u}|\theta) d\mathbf{u} \\ &= \sum_{\mathbf{s}} p(\mathbf{y}, \mathbf{s}|\theta) = \sum_k \alpha_T(k). \end{aligned} \quad (11)$$

As in segmental HMMs, the Viterbi algorithm can be used as a method to segment a waveform by computing the most likely state sequence.

What appears to make the inference in random effects segmental HMMs computationally much more expensive than in segmental HMMs is the inversion of the $d \times d$ covariance matrix of the marginal segment distribution, $\mathbf{X}_r^i \Psi_k \mathbf{X}_r^{i'} + \sigma^2 \mathbf{I}_d$, during the evaluation of the likelihood of a segment. For example, in the F-B algorithm, the likelihood of a segment \mathbf{y}_r^i of length d given state k , $p(\mathbf{y}_r^i | \beta_k, \Psi_k, \sigma^2)$, needs to be calculated for all possible durations d in each of the $\alpha_t(k)$ and $\beta_t(k)$ expressions at each recursion. Naive computation of a segment likelihood, using direct inversion of the $d \times d$ covariance matrix, requires $O(T^3)$ computations, where T is the upper bound for d , leading to an overall time complexity of $O(M^2 T^5)$. This can be computationally impractical for long waveforms with a large value of T (for example, $T = 256$ for the fluid-flow data shown in Figure 1(a)).

In the case of a simpler model with a diagonal covariance matrix for Ψ_k , Holmes and Russell (1999) derived a method for computing the segment likelihood with time complexity $O(M^2 T^3)$. We obtain the same complexity for a more general case with an arbitrary covariance matrix as follows. In discussing computational issues for random effects models, Dempster et al. (1981) suggested an expression for the likelihood that is simple to evaluate. Applying their method to the segment distribution of our model, we rewrite, using Bayes' rule, the likelihood of a segment \mathbf{y}_r^i generated by state k as

$$p(\mathbf{y}_r^i | \beta_k, \Psi_k) = \frac{p(\mathbf{y}_r^i, \mathbf{u}_r^i | \beta_k, \Psi_k, \sigma^2)}{p(\mathbf{u}_r^i | \mathbf{y}_r^i, \beta_k, \Psi_k, \sigma^2)},$$

where the numerator and the denominator of the right-hand side are given as Equations (7) and (8), respectively. The right-hand side of the above equation holds for all values of \mathbf{u}_r^i . By setting \mathbf{u}_r^i to $\hat{\mathbf{u}}_r^i$ as in Equation (9), we can simplify the expression for the segment likelihood to

$$p(\mathbf{y}_r^i | \beta_k, \Psi_k) = (2\pi)^{-d/2} \sigma^{-d} |\Psi_{\hat{\mathbf{u}}_r^i}|^{1/2} / |\Psi_k|^{1/2} \exp(-\mathbf{S}_r^i / (2\sigma^2)), \quad (12)$$

where

$$\mathbf{S}_r^i = (\mathbf{y}_r^i - \mathbf{X}_r^i \beta_k - \mathbf{X}_r^i \hat{\mathbf{u}}_r^i)' (\mathbf{y}_r^i - \mathbf{X}_r^i \beta_k - \mathbf{X}_r^i \hat{\mathbf{u}}_r^i) + \sigma^2 \hat{\mathbf{u}}_r^i{}' \Psi_k^{(-1)} \hat{\mathbf{u}}_r^i.$$

This can be further simplified using Equation (9):

$$\mathbf{S}_r^i = (\mathbf{y}_r^i - \mathbf{X}_r^i \beta_k)' (\mathbf{y}_r^i - \mathbf{X}_r^i \beta_k - \mathbf{X}_r^i \hat{\mathbf{u}}_r^i).$$

Equation (12) has a form that involves only $O(d)$ computations for each step, where previously this involved $O(d^3)$ computations in the case of the naive approach with matrix inversions. Thus, the

time complexities of the F-B and Viterbi algorithms are reduced to $O(M^2T^3)$. For segmental HMMs this computational complexity can be further reduced to $O(M^2T^2)$ by precomputing the segment likelihood and storing the values in a table (Mitchell et al., 1995). However, this precomputation is not possible with random effects models, leading to the additional factor of T in the complexity term.

4.3 Parameter Estimation

In this section, we describe how to obtain maximum-likelihood estimates of the parameters from a training set of multiple waveforms for a random effects segmental HMM using the EM algorithm. We augment the observed waveform data with both (a) state sequences and (b) random effects parameters (both are considered to be hidden). The log likelihood of the complete data of N waveforms, $D_{\text{complete}} = (\mathbf{Y}, \mathbf{S}, \mathbf{U}) = \{(\mathbf{y}^1, \mathbf{s}^1, \mathbf{u}^1), \dots, (\mathbf{y}^N, \mathbf{s}^N, \mathbf{u}^N)\}$, where the state sequence \mathbf{s}^i implies R^i segments in waveform \mathbf{y}^i , is defined as:

$$\begin{aligned} \log L(\theta | D_{\text{complete}}) &= \sum_{i=1}^N \log p(\mathbf{y}^i, \mathbf{s}^i, \mathbf{u}^i | \mathbf{A}, \Lambda, \theta_f) \\ &= \sum_{i=1}^N \sum_{r=1}^{R^i} \log P(s_r^i | s_{r-1}^i, \mathbf{A}) \end{aligned} \quad (13a)$$

$$+ \sum_{i=1}^N \sum_{r=1}^{R^i} \log P(d_r^i | \lambda_k, k = s_r^i) \quad (13b)$$

$$+ \sum_{i=1}^N \sum_{r=1}^{R^i} \log p(\mathbf{y}_r^i | \mathbf{u}_r^i, \beta_k, \sigma^2, k = s_r^i, d_r^i) \quad (13c)$$

$$+ \sum_{i=1}^N \sum_{r=1}^{R^i} \log p(\mathbf{u}_r^i | \Psi_k, k = s_r^i). \quad (13d)$$

As we can see from the above equation, given the complete data, the log-likelihood decouples into four parts Equations (13a)-(13d), where the transition matrix, the duration distribution parameters, the bottom level parameters β_k, σ^2 , and the top level random effect parameters \mathbf{u}_r^i appear in each of the four terms. If we had complete data, we could optimize the four sets of parameters independently. When only parts of the data are observed, by iterating between the E step and the M step in the EM algorithm as described below, we can find a solution that locally maximizes the likelihood of the observed data.

4.3.1 E STEP

In the E step, we find the expected log likelihood of the complete data,

$$Q(\theta^{(t)}, \theta) = E[\log L(\theta | D_{\text{complete}})], \quad (14)$$

with respect to

$$\begin{aligned} p(\mathbf{S}, \mathbf{U} | \mathbf{Y}, \theta^{(t)}) &= p(\mathbf{U} | \mathbf{S}, \mathbf{Y}, \theta^{(t)}) P(\mathbf{S} | \mathbf{Y}, \theta^{(t)}) \\ &= \prod_{i=1}^N \prod_{r=1}^{R^i} p(\mathbf{u}_r^i | s_r^i = k, \mathbf{y}_r^i, \theta^{(t)}) P(s_r^i = k | \mathbf{y}_r^i, \theta^{(t)}), \end{aligned} \quad (15)$$

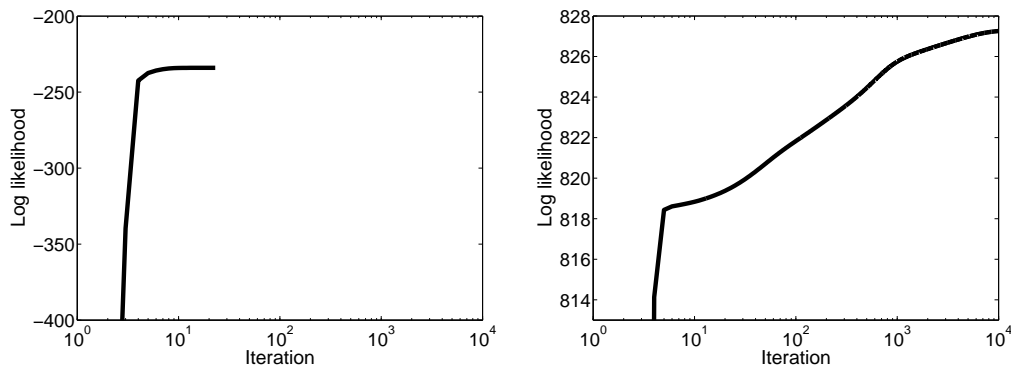


Figure 5: Example of training data log-likelihood convergence as a function of the number of EM iterations, for fluid-flow waveform data, comparing segmental HMMs (on the left) and random effects segmental HMMs (on the right), both using the EM algorithm, x -axis on a log-scale.

where $\theta^{(t)}$ is the estimate of the parameter vector from the previous M step of the t th EM iteration. $P(s_r^i = k | \mathbf{y}_r^i, \theta^{(t)})$ in Equation (15) can be obtained from the F-B algorithm. The sufficient statistics, $E[\mathbf{u}_r^i | s_r^i = k, \mathbf{Y}, \theta^{(t)}]$ and $E[\mathbf{u}_r^i \mathbf{u}_r^{i'} | s_r^i = k, \mathbf{Y}, \theta^{(t)}]$, for $P(\mathbf{u}_r^i | s_r^i = k, \mathbf{y}_r^i, \theta^{(t)})$ in Equation (15) can be directly obtained from Equations (9) and (10). The time complexity for an E step is $O(M^2 T^3 N)$ where N is the number of waveforms (and assuming each waveform is of length T).

4.3.2 M STEP

In the M step, we find the values of the parameters that maximize Equation (14). As we can see from Equations (13a)-(13d) and (14), the optimization problem decouples into four parts, each of which involves a distinct set of parameters. Closed form solutions exist for all of the parameters (the equations are included in Appendix A). The time complexity for each M step is $O(MT^3N)$.

In practice, the algorithm often converges relatively slowly, compared to segmental HMMs, due to the additional missing information in random effects parameters \mathbf{U} . Figure 5 shows a typical run of the algorithm. The segmental HMM converges much faster but converges to a lower log-likelihood value. The iterations were halted when the increase of the log-likelihood from one iteration to the next was less than 10^{-5} .

Holmes and Russell (1999) augmented the observed waveform data with state sequences after integrating out the random effects parameters, and used $D_{\text{complete}} = \{\mathbf{Y}, \mathbf{S}\}$ in the E step. In this case the parameters for the segment distribution $\{\beta_k, \sigma^2, \Psi_k\}$ do not decouple in the complete data log-likelihood and there is no closed form solution for those parameters in the M step. Using the approximate solutions proposed in Holmes and Russell means that the monotonic convergence property of EM is no longer guaranteed. In contrast, if we use $D_{\text{complete}} = \{\mathbf{Y}, \mathbf{S}, \mathbf{U}\}$ in the E step as in Equation (14), we can ensure that the algorithm is a proper EM algorithm that always converges to a local maximum of log likelihood.

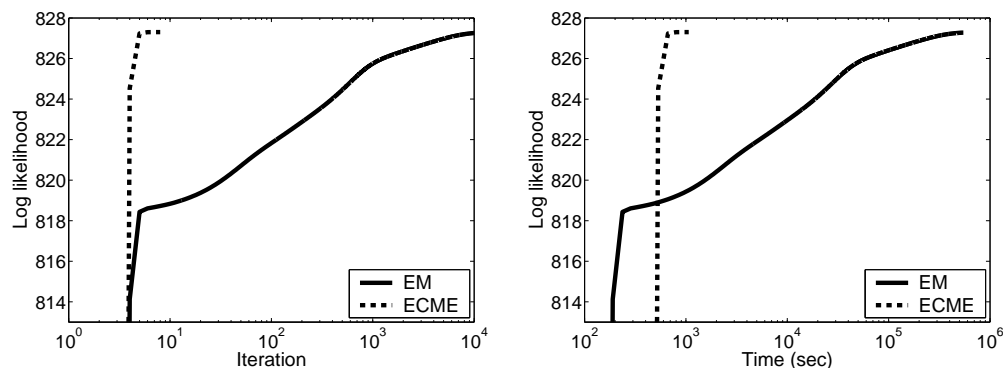


Figure 6: Example of training data log-likelihood convergence as a function of the number of iterations (on the left) and as a function of computation time (on the right), for fluid-flow waveform data (the same data set as in Figure 5), comparing EM vs. ECME for the random effects segmental HMM, x -axis on a log-scale.

4.4 Faster Learning with ECME

As mentioned above, the convergence of the EM algorithm can be very slow especially in the estimation of random effects models. Various extensions of the algorithm have been proposed to speed up the convergence. In the expectation conditional maximization (ECM) algorithm Meng and Rubin (1993) replaced the M step of the EM algorithm with a sequence of $W > 1$ constrained or conditional maximizations (the CM steps). This does not necessarily decrease the number of EM iterations but can significantly reduce the total computation time. Liu and Rubin (1994) further extended the ECM algorithm to the ECME algorithm, reducing both the number of iterations and the total computation time. Both the ECM and the ECME algorithms preserve the property of monotone convergence of the EM algorithm.

More specifically, the CM step of the t th iteration of the ECM algorithm consists of W CM steps. The w th CM step maximizes $Q(\theta^{(t)}, \theta)$ under the constraint

$$g_w(\theta) = g_w(\theta^{(t+(w-1)/W)}),$$

where $\theta^{(t+w/W)}$ denotes the value of θ in the w th CM step of the $(t+1)$ th iteration and $C = \{g_w(\theta), w = 1, \dots, W\}$ is a set of W preselected vector functions. These constraints are set so that the maximization is over the full parameter space of θ . In a typical application of the ECM algorithm the set of parameters θ is divided into W subvectors $\theta_1, \dots, \theta_W$ and in the w th CM step of the t th iteration $Q(\theta^{(t)}, \theta)$ is maximized over θ_w . In this case $g_w(\theta)$ is equal to θ_{-w} , the vector of all parameters except for θ_w . In all of the following discussion we assume $g_w(\theta)$ has this particular form.

In the ECME algorithm some of the CM steps of the ECM algorithm are replaced by a maximization of the actual log likelihood subject to the same constraint instead of the expected complete data log likelihood. The large amount of missing information present in the expected complete data log likelihood leads to slow convergence of the EM algorithm (Dempster et al., 1977). The ECME algorithm often speeds up the convergence dramatically by removing the missing information altogether and maximizing the actual log likelihood in some of the CM steps.

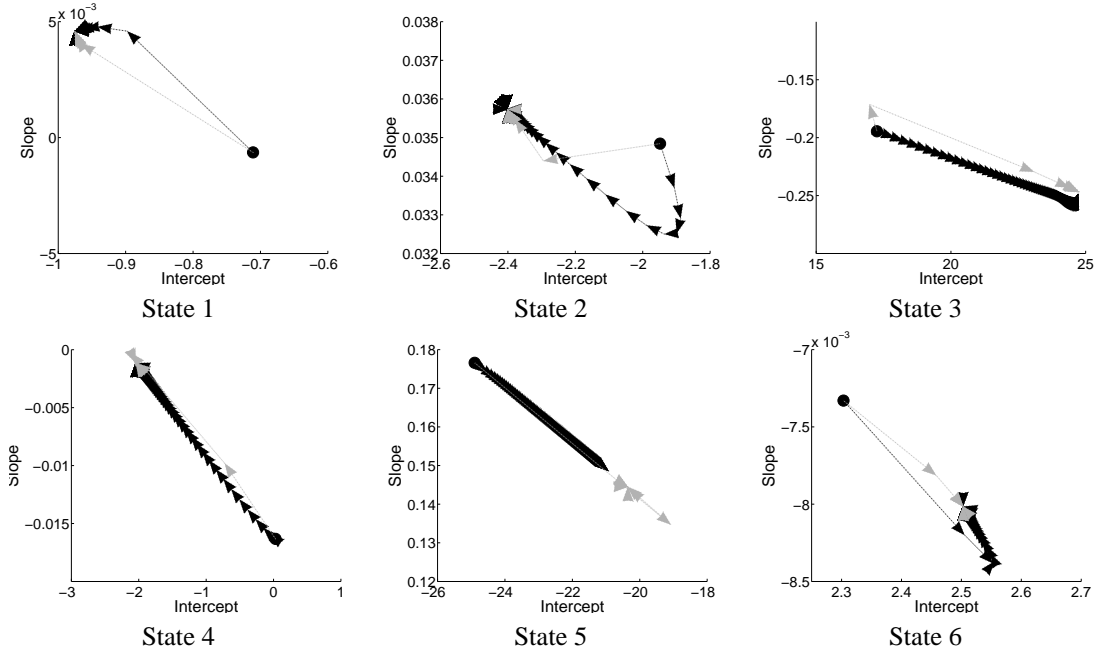


Figure 7: Convergence of β (x -axis is intercept, y -axis is slope) for fluid-flow data. The starting point is indicated by a circle. Gray arrows represent ECME, black arrows represent EM. An arrow for the parameter values is drawn for each iteration in ECME and for every 100 iterations in EM.

Laird and Ware (1982) first derived an ECME algorithm for random effects models but mistakenly thought it was the EM algorithm. Liu and Rubin (1994) gave a formal description of the ECME algorithm and introduced two different versions of the algorithm for random effects models. The first version has a closed form solution in the CM steps. The other requires an iterative algorithm for one of CM steps, and loses the monotone convergence property of the EM algorithm. Liu and Rubin report slightly faster convergence from the latter, but in our application of the ECME algorithm to random effects segmental HMMs we use the first version with closed form CM steps, thus, retaining the monotone convergence property of EM.

For random effects segmental HMMs we partition the parameters θ into $\theta_1 = \{\mathbf{A}, \Lambda, \Psi_k, \sigma^2 | k = 1, \dots, M\}$ and $\theta_2 = \{\beta_k | k = 1, \dots, M\}$ and consider the ECME algorithm with two CM steps for each of the two partitions as follows.

CM step 1: Compute $\mathbf{A}^{(t+1)}$, $\Lambda^{(t+1)}$, $\Psi_k^{(t+1)}$, $k = 1, \dots, M$, and $(\sigma^2)^{(t+1)}$ as in the M step of the EM algorithm.

CM step 2: Given $\Psi_k^{(t+1)}$, $k = 1, \dots, M$, and $(\sigma^2)^{(t+1)}$ obtained from CM Step 1, we can integrate out \mathbf{u}^i from Equations (13c)-(13d), and maximize $\sum_{i=1}^N \sum_{r=1}^{R^i} \log p(\mathbf{y}_r^i | \beta_k, \Psi_k^{(t+1)}, (\sigma^2)^{(t+1)}, k = s_r^i, d_r^i)$, where $p(\mathbf{y}_r^i | \beta_k, \Psi_k^{(t+1)}, (\sigma^2)^{(t+1)}, k = s_r^i, d_r^i)$ is given as

$$N_d(\mathbf{X}_r^i \beta_k, \mathbf{X}_r^i \Psi_k^{(t+1)} \mathbf{X}_r^{i'} + (\sigma^2)^{(t+1)} \mathbf{I}_d).$$

The update equations for $\beta_k^{(t+1)}$, $k = 1, \dots, M$ are

$$\beta_k^{(t+1)} = \left(\sum_{i=1}^N \frac{\sum_t \sum_{d < t} C_{iktd}(\mathbf{X}_{td}^i \mathbf{Z}_{td}^i \mathbf{X}_{td}^i)}{P(\mathbf{y}^i | \boldsymbol{\theta}^{(t)})} \right)^{-1} \cdot \left(\sum_{i=1}^N \frac{\sum_t \sum_{d < t} C_{iktd}(\mathbf{X}_{td}^i \mathbf{Z}_{td}^i \mathbf{y}_{td}^i)}{P(\mathbf{y}^i | \boldsymbol{\theta}^{(t)})} \right),$$

where $\mathbf{X}_{td}^i = \mathbf{X}_{t-d+1:t}^i$ and

$$\mathbf{Z}_{td}^i = (\mathbf{X}_{td}^i \boldsymbol{\Psi}_k^{(t+1)} \mathbf{X}_{td}^{i'} + (\sigma^2)^{(t+1)} \mathbf{I}_d)^{-1}.$$

When d is large we can avoid inverting a $d \times d$ matrix to obtain \mathbf{Z}_{td}^i by rewriting this as

$$\mathbf{Z}_{td}^i = \{ \mathbf{I}_d - \mathbf{X}_{td}^i ((\sigma^2)^{(t+1)} (\boldsymbol{\Psi}_k)^{-1} + \mathbf{X}_{td}^i \mathbf{X}_{td}^i)^{-1} \mathbf{X}_{td}^i \} / (\sigma^2)^{(t+1)}.$$

CM step 1 maximizes the expected complete data log likelihood where both state sequences \mathbf{S} and random effects parameters \mathbf{U} are considered missing. In CM step 2 the incomplete data log likelihood is augmented only with \mathbf{S} and then maximized. The computational complexity of the update equation for $\beta_k^{(t+1)}$ in CM step 2 is $O(MT^4N)$ compared to $O(MT^3N)$ for the same parameter in the M step of the EM algorithm. Thus, the overall asymptotic complexity for the CM steps is $O(MT^4N)$, and the ECME algorithm is computationally more expensive in time complexity per iteration than the EM algorithm.

The convergence of the EM and the ECME algorithms for a random effects segmental HMM with six states is shown in Figure 6 for the fluid-flow waveform data described in Section 5.1. The parameters were initialized to the same values for both algorithms and the convergence criterion was set to 10^{-5} . In Figure 6(a) the EM algorithm takes 11506 iterations to converge to roughly the same log-likelihood that the ECME algorithm converges to in only 8 iterations. Each iteration takes 133.3s in the ECME algorithm, versus 47.4s in the EM algorithm, but the overall time to convergence of ECME is still over 3 orders of magnitude faster than EM (as shown in Figure 6(b)).

The convergence trajectories of the 2-dimensional parameters β_k for both algorithms are shown in Figure 7 for each of the six states. The starting values are shown as black circles. Black arrows represent the parameter values of every 100 iterations in the EM algorithm and grey arrows represent the parameters in every iteration of the ECME algorithm. Both Figure 6 and Figure 7 show a dramatic improvement in the speed of convergence of ECME over EM: they both converge to the same solutions in parameter space but ECME converges much more quickly.

5. Experiments

We apply our model to two real-world data sets: (a) hot-film anemometry data in turbulent bubbly fluid-flow and (b) ECG heartbeat data: both are described in more detail below in Section 5.1. In all of our experiments we compare the results from our new segmental HMM with random effects to those obtained using segmental HMMs without random effects. We use several methods to evaluate the models:

Average LogP Score: We compute $\log p(\mathbf{y} | \boldsymbol{\theta})$ scores (Equations (4) and (11) for each model) for test waveforms \mathbf{y} to compare how much probability is assigned to new test data by different models. Higher logP scores indicate better predictive power.

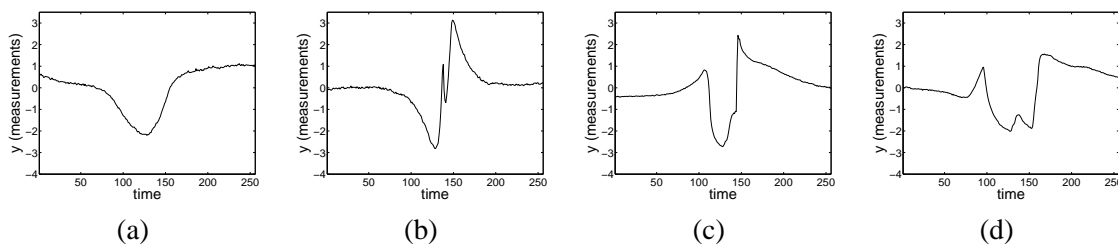


Figure 8: Negative examples in bubble-probe interaction data. (a) no interaction (b) glancing (c) bouncing (d) penetrating.

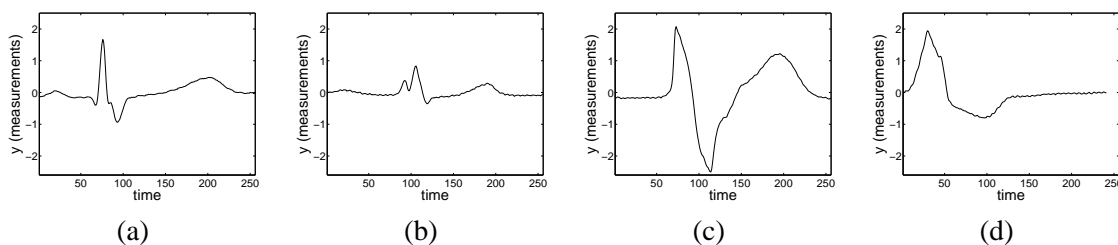


Figure 9: Negative examples in ECG data (a) right bundle branch block beat (b) left bundle branch block beat (c) paced beat (d) premature ventricular contraction beat.

Segmentation Quality: To evaluate how well the model can segment test waveforms, we first obtain the segmentations of test waveforms with the Viterbi algorithm, estimate the regression coefficients $\hat{\gamma}$ of each segment, and calculate the mean squared difference between the observed data and $\mathbf{X}\hat{\gamma}$. Good segmentations should produce low scores.

Recognition Accuracy: We use the model learned from a training set of positive examples to recognize waveforms of interest from a test set with both positive and negative exemplars. We compare the results from random effects segmental HMMs with those from dynamic time warping (Keogh and Pazzani, 2000), Euclidean distance matching, and segmental HMMs.

All of the experiments were conducted using cross-validation. The number of segments M for each data set was determined by visual inspection prior to training the models. All waveforms were shifted to have zero mean amplitude before training and testing.

In all experiments reported below, we use the ECME algorithm for training random effects segmental HMMs. The convergence criterion is set to 10^{-5} . We found in our experiments that providing one manually-segmented example is useful in initialization of both EM and ECME—details on initialization are described in Appendix B.

5.1 Data Sets

Below we describe two different data sets that were used as the basis for our experiments.

	Bubble-probe interaction data		ECG data	
	Avg. LogP Score	Avg. Segmentation Error	Avg. LogP Score	Avg. Segmentation Error
Segmental HMMs	-3.25	15.39	-3.12	2.55
Random Effects Segmental HMMs	4.50	1.43	19.63	0.39

Table 1: Average logP scores and segmentation errors for bubble-probe interaction data and ECG data.

5.1.1 BUBBLE-PROBE INTERACTION DATA

Hot-film anemometry is a technique commonly used in turbulent bubbly flow measurements in fluid physics. Different types of interactions between the bubbles and the probe in turbulent gas flow, such as splitting, bouncing, and penetration, lead to characteristic waveform shapes. Automatically detecting the occurrence and types of interactions from such waveforms is a problem of active interest (Bruun, 1995). This recognition task is difficult because of the large variability in the shapes of waveforms within a given class of interactions (e.g., Figure 1(b)), caused by various factors such as velocity fluctuations and different gas fractions during measurement.

We applied our method to individual bubble-probe interaction data. Our data set consisted of 7 waveforms in the class *no interaction* (Figure 8(a)), 5 waveforms in the class *glancing* (Figure 8(b)), 52 waveforms in the class *bouncing* (Figure 8(c)), 8 waveforms in the class *penetration* (Figure 8(d)) and 48 waveforms in the class *splitting* (Figures 1(a) and (b)). Class labels were determined for each interaction based on expert examination of high-speed image recordings of the event obtained simultaneously with the interaction signal (Luther, 2004). Each waveform had 256 data points sampled at 5kHz. We built waveform models for the class of *splitting* interactions, where the probe splits the bubble, and ran a 9-fold cross-validation with 5 waveforms in the training set and 43 waveforms in the test set for each run. The 72 waveforms from the other interactions were used as negative examples in the test set. Given that Figure 2(a) is a reasonable piecewise linear approximation of the general shape, we subjectively chose $M = 6$ as the number of states for both segmental HMMs and random effects segmental HMMs.

5.1.2 ECG DATA

The shape of heartbeat cycles in ECG data can be used to diagnose the heart condition of a patient (Koski, 1996; Hughes et al., 2003). For example, Figure 11 shows the typical shape of normal heartbeats, whereas Figures 9(a)-(d) are taken from a heart experiencing various abnormal conditions. Heartbeats of the same type can vary significantly across individuals in terms of the heights and locations of peaks in the shape. Variability can also be found among heartbeats from the same individual although it is lower than across individuals.

For our experiments we used the ECG recordings with a sampling rate of 360 samples per second from the MIT-BIH Arrhythmia database¹. We selected hour long recordings from 23 subjects and manually extracted two heartbeats of the same type from each subject. Normal heartbeats were

1. <http://www.physionet.org/physiobank/database/mitdb/>

	Top 10	Top 20
Euclidean distance (using mean distance)	86.7	81.7
Euclidean distance (using minimum distance)	82.2	80.0
Dynamic time warping (using mean distance)	85.6	82.2
Dynamic time warping (using minimum distance)	92.2	82.8
Segmental HMMs	86.7	82.2
Random Effects Segmental HMMs	100.0	95.0

Table 2: Cross-validated recognition accuracy for bubble-probe interaction data on test set. The numbers represent the true positive rates in percentages (%) among the top k waveforms selected by each algorithm.

taken from each of twelve subjects, and similarly, left bundle branch block beats from three subjects, right bundle branch block beats from two subjects, premature ventricular contraction beats from three subjects, and paced beats from three subjects. The lengths of heartbeats varied approximately from 210 to 410 samples. We modeled each normal heartbeat with $M = 9$ segments. We performed a 4-fold cross-validation with 6 normal waveforms from three individuals as a training set for each cross-validation run and the remainder as a test set. Note that the test set contained heartbeats from a different set of individuals than the individuals used to train the model. Segmental HMMs could not be learned for one of the cross-validation runs due to numerical instability (a problem that did not occur with random effects HMMs), so we report results from the remaining three runs of cross-validations for segmental HMMs. The 22 abnormal heartbeats were used as negative examples for the evaluation of recognition accuracy in the test sets.

5.2 Results

In Table 1 we compare the average logP scores of positive test waveforms for segmental HMMs with those for random effects segmental HMMs. The new model produces significantly higher scores for both data sets, indicating that random effects allow segmental HMMs to capture both the typical shape and shape variability.

Table 1 also shows the average segmentation errors for the test waveforms from both models. Adding the random effects component to segmental HMMs reduces the segmentation error roughly by a factor of 10 on both data sets. Segmentation examples are shown in Figure 10 for the bubble-probe interaction data and Figure 11 for the ECG data, where it is apparent that random effects segmental HMMs are more consistent in locating segment boundaries.

To evaluate the recognition accuracy we score both pattern and non-pattern waveforms in the test set using the model for the pattern waveform learned from the training set, and rank the waveforms according to their log probability scores. We also compare probabilistic methods with non-probabilistic scoring methods such as Euclidean distance and dynamic time warping. For non-probabilistic methods we compute the distance between a test waveform and each of the N training waveforms, and use both the average and minimum of the N distances as a score for that test waveform. The percentages of the true positives in the top 10 and 20 waveforms from bubble-probe interaction data are reported in Table 2. Random effects segmental HMMs give a substantially

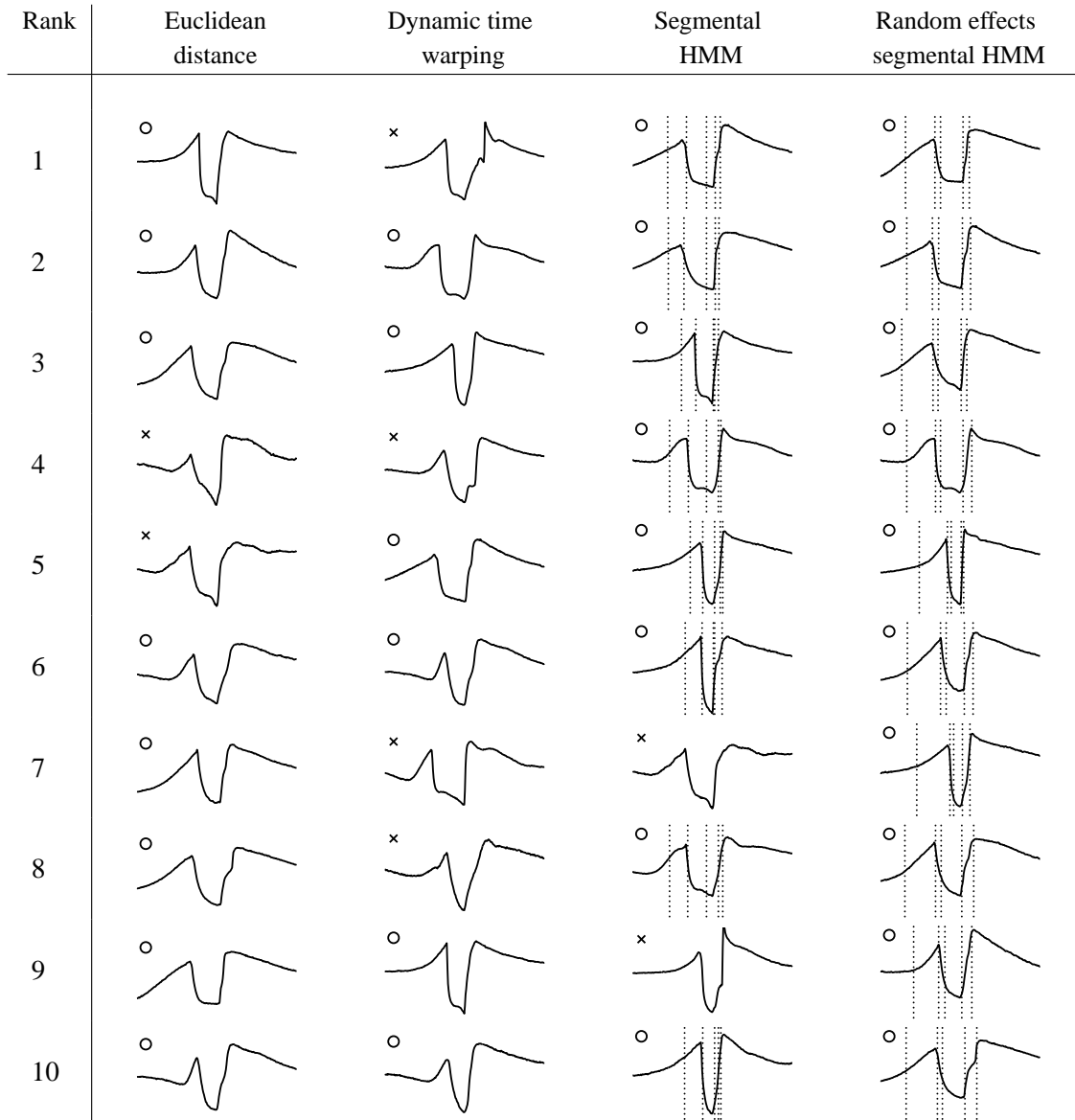


Figure 10: Top 10 waveforms found by four different algorithms in bubble-probe interaction data. ‘o’s are true positives and ‘x’s are false positives. Segmentations by the Viterbi algorithm are overlaid on top of the waveforms in the case of true positives for segmental HMMs and random effects segmental HMMs. Segmentations are not produced by the Euclidean distance method or by dynamic time warping.

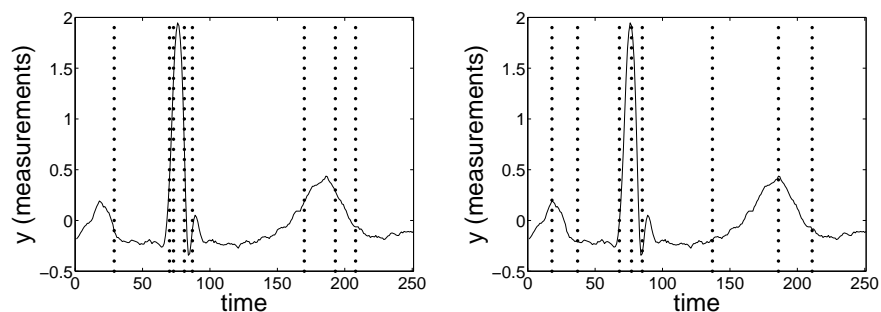


Figure 11: Segmentation of a normal ECG heartbeat by the Viterbi algorithm for segmental HMMs (left) and for random effects segmental HMMs (right).

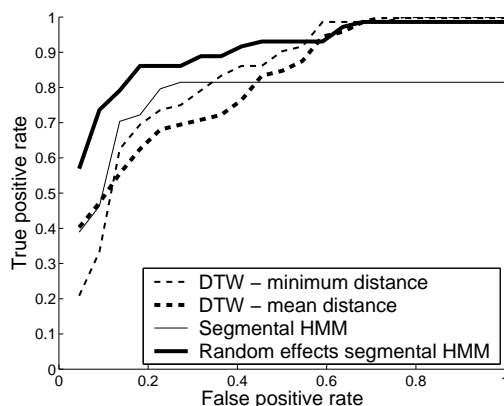


Figure 12: ROC plot for ECG data.

higher accuracy than any of the other methods. Figure 10 shows the top 10 waveforms found by the different methods. All of the false positives are from the interaction class *bouncing*, which is more similar in shape to the class *splitting* than other interaction types. Random effects segmental HMMs can effectively distinguish subtle differences in shape between the pattern that we are modeling and the non-pattern waveforms. Segmentations are overlaid in Figure 10 on the waveforms as found by probabilistic models using the Viterbi algorithm. Such segmentations are not available for dynamic time warping and Euclidean distance methods, providing an additional advantage of using probabilistic models in applications where segmentation is useful.

Figure 12 shows the ROC curves for the ECG data. The results from Euclidean distance are not available for ECG data because the method as implemented requires the length of each waveform sequence to be the same. Random effects segmental HMMs have the highest accuracy, particularly over the range from 0 to 0.5 in terms of fraction of false positives (x -axis) which is typically the range of interest when ranking objects by similarity to a target. A similar result was obtained for bubble-probe interaction data as can be seen in Figure 13.

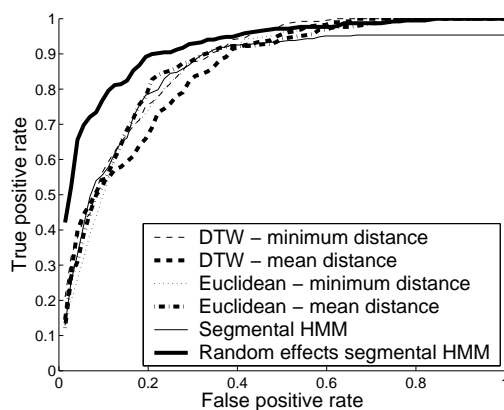


Figure 13: ROC plot for bubble-probe interaction data.

6. Discussions and Conclusions

As noted elsewhere in the paper, the random effects segmental HMM proposed in this paper can be extended in multiple different ways. For example, the parametrization of the segment models as linear functions of time can be generalized directly to any functional form that is linear in the parameters without altering the underlying time complexity of the learning and inference algorithms.

In the results reported here we applied our model to score relatively short waveform “snippets” to detect waveforms that are similar in shape to a query waveform. In order to parse online time-series data and detect “embedded” waveforms relative to a target, a two-state HMM with a pattern state and a background state can be used, where the random effects segmental HMM is embedded inside the pattern state. Each instance of the pattern waveform is allowed to have its own parameters via the random effects mechanism. The background state models any measurements that do not belong to pattern waveforms. A long time-series can then be parsed via the Viterbi algorithm (for example) to segment the series into background and pattern states, where the segments that belong to the pattern state correspond to predicted waveform locations according to the model.

In conclusion, we have proposed a probabilistic model that extends segmental HMMs to include random effects. This model allows an individual waveform to vary its shape in a constrained manner via a prior distribution over individual waveform parameters. The ECME algorithm for learning this model greatly improved the speed of convergence of parameter estimation compared to a standard EM approach. Experimental results support the hypothesis that random effects segmental HMMs perform better in modeling, segmentation, and recognition of waveforms compared both to probabilistic models without random effects and to non-probabilistic methods.

Acknowledgments

This material is based upon work supported by the National Science Foundation under award numbers SCI-0225642 and IIS-0431085. We also thank David Van Dyk for discussions relating to random effects models and EM, Stefan Luther for providing the fluid-flow waveform data, and the referees for providing useful comments that improved the presentation of the paper.

Appendix A: Re-estimation Formulas for EM

The re-estimation formula for the transition probabilities and the duration distribution parameters can be shown to be:

$$a_{kl}^{(t+1)} = \frac{\sum_{i=1}^N \frac{1}{P(\mathbf{y}^i | \boldsymbol{\theta}^{(t)})} \sum_t \alpha_t^i(k) a_{kl}^{(t)} \beta_t^{i*}(l)}{\sum_{i=1}^N \frac{1}{P(\mathbf{y}^i | \boldsymbol{\theta}^{(t)})} \sum_m \sum_t \alpha_t^i(k) a_{km}^{(t)} \beta_t^{i*}(l)},$$

$$\lambda_k^{(t+1)} = \frac{\sum_{i=1}^N \frac{1}{P(\mathbf{y}^i | \boldsymbol{\theta}^{(t)})} \sum_t \sum_d C_{iktd} \cdot (d-1)}{\sum_{i=1}^N \frac{1}{P(\mathbf{y}^i | \boldsymbol{\theta}^{(t)})} \sum_t \sum_d C_{iktd}},$$

where

$$C_{iktd} = \alpha_t^{i*}(k) P(d | \lambda_k^{(t)}) P(\mathbf{y}_{t+1:t+d}^i | \boldsymbol{\theta}_{f_k}^{(t)}) \beta_{t+d}^{i*}(k).$$

Using the notation of $\mathbf{X}_{td}^i = \mathbf{X}_{t-d+1:t}^i$ and $\mathbf{y}_{td}^i = \mathbf{y}_{t-d+1:t}^i$, we update the covariance matrix of the top level of the segment distribution model according to

$$\Psi_k^{(t+1)} = \frac{\sum_{i=1}^N \frac{\sum_t \sum_{d < t} C_{iktd} E[\mathbf{u}_k^i \mathbf{u}_k^{i'} | \mathbf{Y}, \boldsymbol{\theta}^{(t)}]}{P(\mathbf{y}^i | \boldsymbol{\theta}^{(t)})}}{\sum_{i=1}^N \frac{\sum_t \sum_{d < t} C_{iktd}}{P(\mathbf{y}^i | \boldsymbol{\theta}^{(t)})}},$$

and for the bottom level, we re-estimate the parameters using

$$\beta_k^{(t+1)} = \left(\sum_{i=1}^N \frac{\sum_t \sum_{d < t} C_{iktd} (\mathbf{X}_{td}^i \mathbf{X}_{td}^i)'}{P(\mathbf{y}^i | \boldsymbol{\theta}^{(t)})} \right)^{-1} \cdot \left(\sum_{i=1}^N \frac{\sum_t \sum_{d < t} C_{iktd} (\mathbf{X}_{td}^i (\mathbf{y}_{td}^i - \mathbf{X}_{td}^i \beta_k - \mathbf{X}_{td}^i E[\mathbf{u}_k^i | \mathbf{Y}, \boldsymbol{\theta}^{(t)}]))'}{P(\mathbf{y}^i | \boldsymbol{\theta}^{(t)})} \right)$$

$$(\sigma^2)^{(t+1)} = \frac{\sum_{i=1}^N \frac{\sum_{k=1}^M \sum_t \sum_{d < t} C_{iktd} E[\mathbf{D}_k^i \mathbf{D}_k^i | \mathbf{Y}, \boldsymbol{\theta}^{(t)}]}{P(\mathbf{y}^i | \boldsymbol{\theta}^{(t)})}}{\sum_{i=1}^N \frac{\sum_{k=1}^M \sum_t \sum_{d < t} C_{iktd} d}{P(\mathbf{y}^i | \boldsymbol{\theta}^{(t)})}},$$

where

$$E[\mathbf{D}_k^i \mathbf{D}_k^i | \mathbf{Y}, \boldsymbol{\theta}^{(t)}] = (\mathbf{y}_{t+1:t+d}^i - \mathbf{X}_{td}^i \beta_k - \mathbf{X}_{td}^i E[\mathbf{u}_k^i | \mathbf{Y}, \boldsymbol{\theta}^{(t)}])' \cdot (\mathbf{y}_{td}^i - \mathbf{X}_{td}^i \beta_k - \mathbf{X}_{td}^i E[\mathbf{u}_k^i | \mathbf{Y}, \boldsymbol{\theta}^{(t)}])$$

$$+ \text{tr}[\mathbf{X}_{td}^i \mathbf{X}_{td}^i \text{Var}(\mathbf{u}_k^i | \mathbf{Y}, \boldsymbol{\theta}^{(t)})].$$

Appendix B: Initialization of the EM and ECME Algorithms

Initialization of the EM and ECME algorithms is based on manual segmentation of a single waveform in the training data. The manual segmentation is only used to determine initial values for the parameters (for use in the first E-step), and is not used in any further manner by EM or ECME after this initialization.

Given the manually segmented waveform, the parameters \mathbf{A} , θ_d , and β_k 's are set to their maximum-likelihood values as estimated from this waveform. The 2×2 covariance matrices Ψ_k 's of the random effects component of the model require more than two segmented waveforms in order to obtain maximum-likelihood estimates—thus, their values are initialized in a different manner as follows. The variance term for the slope in Ψ_k 's is set to a value generated from a uniform distribution over $[z_{\min}, z_{\max}]$. From preliminary inspection of data z_{\min} and z_{\max} are set to 1 and 10 respectively for bubble-probe interaction data, and 1 and 5 for ECG data. As the state index increases, the values of the intercept parameters in β_k 's tend to increase and a small variability in slope leads to a more significant variability in intercept values. To take into account this we initialize the variance for the intercept by sampling a value from the same uniform distribution $[z_{\min}, z_{\max}]$ and multiplying this value by the state index i for that intercept. Given that a positive change in the slope leads to a decreased value of the intercept we initialize the covariance between the slope and intercept to a negative value generated from a uniform distribution over $[z_{\min} \times (-0.1), z_{\max} \times (-0.1)]$. Multiplying z_{\min} and z_{\max} by 0.1 makes the covariance relatively small compared to variances in Ψ_k 's and also ensures that the covariance matrices Ψ_k 's are positive definite. Finally, we sample the initial value for the noise parameter σ^2 from a uniform distribution over $[1, 6]$ for both data sets. This initialization strategy essentially sets the variance parameters Ψ_k 's and σ^2 to relatively large initial values and then lets them adjust to the training data.

References

- Kannan Achan, Sam Roweis, Aaron Hertzmann, and Brendan Frey. A segment-based probabilistic generative model of speech. In *Proc. of the 2005 IEEE International Conference on Acoustics, Speech, and Signal Processing*, volume 5, pages 221–224, Philadelphia, PA, 2005. IEEE.
- Rakesh Agrawal, Christos Faloutsos, and Arun N. Swami. Efficient similarity search in sequence databases. In *Proc. of the 4th International Conference of Foundations of Data Organization and Algorithms*, pages 69–84, Chicago, IL, 1993. Springer Verlag.
- Theron Bennett and John Murphy. Analysis of seismic discrimination using regional data from western United States events. *Bull. Seis. Soc. Am.*, 76:1069–1086, 1986.
- Hans Bruun. *Hot Wire Anemometry: Principles and Signal Analysis*. Oxford University Press, Oxford, 1995.
- King-pong Chan and Ada Wai-chee Fu. Efficient time series matching by wavelets. In *Proc. of the 15th International Conference on Data Engineering*, pages 126–133, Sydney, Australia, 1999. IEEE Computer Society.
- Arthur Dempster, Nan Laird, and Donald Rubin. Maximum likelihood estimation from incomplete data via the EM algorithm. *Journal of the Royal Statistical Society Series B*, 39:1–38, 1977.
- Arthur Dempster, Donald Rubin, and Robert Tsutakawa. Estimation in covariance components models. *Journal of the American Statistical Association*, 76(374):341–353, 1981.
- Li Deng, Mike Aksmanovic, Xiaodong Sun, and Jeff Wu. Speech recognition using hidden Markov models with polynomial regression functions as nonstationary states. *IEEE Trans. Speech Audio Processing*, 2(4):507–520, 1994.

- James Ferguson. Variable duration models for speech. In *Proc. of the Symposium on the Application of Hidden Markov Models to Text and Speech*, pages 143–179, Princeton, NJ, 1980. IDA-CRD.
- Mark Gales and Steve Young. The theory of segmental hidden Markov models. Technical Report CUED/F-INFENG/TR 133, Cambridge University Engineering Department, 1993.
- Xianping Ge and Padhraic Smyth. Deformable Markov model templates for time-series pattern matching. In *Proc. of the 6th ACM SIGKDD International Conference on Knowledge Discovery and Data Mining*, pages 81–90, Boston, MA, 2000. ACM Press.
- Wendy Holmes and Martin Russell. Probabilistic-trajectory segmental HMMs. *Computer Speech and Language*, 13(1):3–37, 1999.
- Nicholas Hughes, Lionel Tarassenko, and Stephen Roberts. Markov models for automated ECG interval analysis. In *Advances in Neural Information Processing Systems 16*, pages 611–618, Cambridge, MA, 2003. MIT Press.
- Stanislaw Jankowski and Artur Oreziak. Learning system for computer-aided ECG analysis based on support vector machines. *International Journal of Bioelectromagnetism*, 5(1):175–176, 2003.
- Michael Jordan, editor. *Learning in Graphical Models*. MIT Press, Cambridge, MA, 1999.
- Eamonn Keogh and Michael Pazzani. Scaling up dynamic time warping for datamining applications. In *Proc. of the 6th ACM SIGKDD International Conference on Knowledge Discovery and Data Mining*, pages 285–289, Boston, MA, 2000. ACM Press.
- Eamonn Keogh and Padhraic Smyth. A probabilistic approach to fast pattern matching in time series databases. In *Proc. of the 3rd ACM SIGKDD International Conference on Knowledge Discovery and Data Mining*, pages 24–30, Newport Beach, CA, 1997. AAAI Press.
- Seyoung Kim, Padhraic Smyth, and Stefan Luther. Modeling waveform shapes with random effects segmental hidden Markov models. In *Proc. of the 20th International Conference on Uncertainty in AI*, pages 309–316, Banff, Canada, 2004. AUAI Press.
- Antti Koski. Modelling ECG signals with hidden Markov models. *Artificial Intelligence in Medicine*, 8(5):453–471, 1996.
- Nan Laird and James Ware. Random-effects models for longitudinal data. *Biometrics*, 38(4):963–974, 1982.
- Nan Laird, Nicholas Lange, and Daniel Stram. Maximum likelihood computations with repeated measures: application of the EM algorithm. *Journal of the American Statistical Association*, 82(397):97–105, 1987.
- Stephen Levinson. Continuously variable duration hidden Markov models for automatic speech recognition. *Computer Speech and Language*, 1(1):29–45, 1986.
- Chuanhai. Liu and Donald Rubin. The ECME algorithm: a simple extension of EM and ECM with faster monotone convergence. *Biometrika*, 81(4):633–648, 1994.
- Stefan Luther, 2004. personal correspondence.

- Xiao-Li Meng and Donald Rubin. Maximum likelihood estimation via the ECM algorithm: a general framework. *Biometrika*, 80:267–278, 1993.
- Carl Mitchell, Mary Harper, and Leah Jamieson. On the computational complexity of explicit duration HMMs. *IEEE Trans. on Speech and Audio Processing*, 3(3):213–217, 1995.
- Kevin Murphy. *Dynamic Bayesian Networks: Representation, Inference, and Learning*. PhD thesis, University of California, Berkeley, 2002.
- Mari Ostendorf, Vassilios Digalakis, and Owen Kimball. From HMMs to segmental models: a unified view of stochastic modeling for speech recognition. *IEEE Trans. on Speech and Audio Processing*, 4(5):360–378, 1996.
- Lawrence Rabiner and Bing-Hwang Juang. *Fundamentals of Speech Recognition*. Prentice Hall, Englewood Cliffs, NJ, 1993.
- Martin Russell. A segmental HMM for speech pattern matching. In *Proc. of the 1993 IEEE International Conference on Acoustics, Speech and Signal Processing*, pages 499–502, Minneapolis, MN, 1993. IEEE.
- Martin Russell and Roger Moore. Explicit modeling of state occupancy in hidden Markov models for automatic speech recognition. In *Proc. of the 1985 IEEE International Conference on Acoustics, Speech and Signal Processing*, pages 2376–2379, Tampa, FL, 1985. IEEE.
- Shayle Searle, George Casella, and Charles McCulloch. *Variance Components*. Wiley, New York, 1992.
- Yair Shimshoni and Nathan Intrator. Classification of seismic signals by integrating ensembles of neural networks. *IEEE Trans. on Signal Processing*, 46:1194–1201, 1998.
- Byoung-Kee Yi and Christos Faloutsos. Fast time sequence indexing for arbitrary L_p norms. In *Proc. of the 26th Very Large Data Bases Conference*, pages 385–394, Cairo, Egypt, 2000. Morgan Kaufmann.
- Young-Sun Yun and Yung-Hwan Oh. A segmental-feature HMM for speech pattern modeling. *IEEE Signal Processing Letters*, 7(6):135–137, 2000.